Binding of Salicylhydroxamic Acid and Several Aromatic Donor Molecules to *Arthromyces ramosus* Peroxidase, Investigated by X-ray Crystallography, Optical Difference Spectroscopy, NMR Relaxation, Molecular Dynamics, and Kinetics[†,‡]

Kikuo Tsukamoto,[$] Hiroyuki Itakura,[§] Koichi Sato,[||] Keiichi Fukuyama,[§] Shigetoshi Miura,[⊥] Seizo Takahashi,[@] Hiroh Ikezawa,[$] and Toichiro Hosoya*[,#]

Department of Microbial Chemistry, Faculty of Pharmaceutical Sciences, Nagoya City University, Nagoya 467-8603, Japan, Department of Biology, Graduate School of Science, Osaka University, Toyonaka 560-0043, Japan, Chiba University School of Medicine, Chiba 260-8670, Japan, Department of Biological Science and Technology, Science University of Tokyo, Noda 278-0022, Japan, Faculty of Science, Japan Women's University, Tokyo 112-0015, Japan, and Department of Biochemistry, Dokkyo University Medical School, Mibu 321-0202, Japan

Received December 11, 1998; Revised Manuscript Received July 2, 1999

ABSTRACT: The X-ray crystal structure of the complex of salicylhydroxamic acid (SHA) with *Arthromyces ramosus* peroxidase (ARP) has been determined at 1.9 Å resolution. The position of SHA in the active site of ARP is similar to that of the complex of benzhydroxamic acid (BHA) with ARP [Itakura, H., et al. (1997) *FEBS Lett. 412*, 107−110]. The aromatic ring of SHA binds to a hydrophobic region at the opening of the distal pocket, and the hydroxamic acid moiety forms hydrogen bonds with the His56, Arg52, and Pro154 residues but is not asscoiated with the heme iron. X-ray analyses of ARP−resorcinol and ARP−*p*-cresol complexes failed to identify the aromatic donor molecules, most likely due to the very low affinities of these aromatic donors for ARP. Therefore, we examined the locations of these and other aromatic donors on ARP by the molecular dynamics method and found that the benzene rings are trapped similarly by hydrophobic interactions with the Ala92, Pro156, Leu192, and Phe230 residues at the entrance of the heme pocket, but the dihedral angles between the benzene rings and the heme plane vary from donor to donor. The distances between the heme iron and protons of SHA and resorcinol are similar to those obtained by NMR relaxation. Although SHA and BHA are usually considered potent inhibitors for peroxidase, they were found to reduce compound I and compound II of ARP and horseradish peroxidase C in the same manner as *p*-cresol and resorcinol. The aforementioned spatial relationships of these aromatic donors to the heme iron in ARP are discussed with respect to the quantum chemical mechanism of electron transfer in peroxidase reactions.

Heme-containing peroxidases are a family of enzymes that catalyze the oxidation of many organic and inorganic compounds at the expense of hydrogen peroxide or organic oxide (*1*−*3*). Oxidation of aromatic compounds (AH_2) occurs through the following scheme:

$$E + H_2O_2 \xrightarrow{k_1} \text{cpd I} + H_2O \quad (1)$$

$$\text{cpd I} + AH_2 \xrightarrow{k_2} \text{cpd II} + AH^{\bullet} \quad (2)$$

$$\text{cpd II} + AH_2 \xrightarrow{k_3} E + AH^{\bullet} + H_2O \quad (3)$$

$$AH^{\bullet} + AH^{\bullet} \rightarrow A_2H_2 \text{ or } A + AH_2 \quad (4)$$

where E is the enzyme in the resting state and compound I (cpd I)[1] and cpd II are intermediates that have two and one higher oxidation equivalent than the resting state, respectively. AH_2 is the organic electron donor molecule, and $AH^{\bullet}$ is its radical that produces the final product through a nonenzymatic reaction such as disproportionation or polymerization.

It is known that eqs 2 and 3 are single-electron transfer reactions; the latter is the rate-limiting step. Little is known about the mechanism of electron transfer during these reactions. Reactions 2 and 3 are second-order, but there are some reports demonstrating saturation by the substrate in these reactions (*4*−*7*). This suggests that the electron transfer may occur in complexes that bind the substrates at a defined place.

It is, however, almost impossible to study physicochemically the features of complexes of the cpd I and cpd II with aromatic electron donor molecules because the lifetime of the complexes is too short. If the locations of donors on cpd

[†] This work was supported in part by a Grants-in-Aid for Scientific Research on Priority Areas (Molecular Biometallics) (Grants 09235217 and 10129219 to K.F. and Grant 08249237 to S.M.) from the Ministry of Education, Science and Culture of Japan.

[‡] The atomic parameters of the ARP−SHA complex (file name 1ck6) have been deposited in the Protein Data Bank, Brookhaven National Laboratory, Upton, NY.

* To whom correspondence should be addressed: 4-27-7 Tsuganodai, Wakaba-ku, Chiba 264-0033, Japan (home address). Telephone and fax: +81-043-255-8228. E-mail: t-hosoya@sa2.so-net.ne.jp.

[$] Nagoya City University.

[§] Osaka University.

[||] Chiba University School of Medicine.

[⊥] Science University of Tokyo.

[@] Japan Women's University.

[#] Dokkyo University Medical School.

[1] Abbreviations: ARP, *Arthromyces ramosus* peroxidase; BHA, benzhydroxamic acid; CCP, cytochrome *c* peroxidase; cpd I, compound I; cpd II, compound II; 6c, six-coordinate; HS, high-spin; HOMO, highest occupied molecular orbital; HRP, horseradish peroxidase; HRPC, horseradish peroxidase isozyme C; LUMO, lowest occupied molecular orbital; MD, molecular dynamics; MPO, myeloperoxidase; NOE, nuclear Overhauser effect; SHA, salicylhydroxamic acid.

10.1021/bi982925l CCC: $18.00
Published on Web 09/10/1999

I and cpd II are the same as those on the resting form of the enzyme, studies of the locations of donors on the resting enzyme become significant in the study of the electron transfer mechanism. Accordingly, the binding of various donors to HRP has been studied by NMR, optical difference spectrum, and other methods (*8*−*10*). Evidence has been obtained by physicochemical methods showing that the native enzyme interacts with aromatic donors to form a 1:1 complex. NOE (*8*, *11*) and chemical modification (*12*) showed that protons of BHA and other donors are located close to heme methyl C18H_3 and δ-meso proton C20H. Further studies of the precise binding sites and binding mode were difficult due to the lack of HRP with a high-resolution structure. Therefore, several groups developed modeling and MD procedures for locating the aromatic donors on HRP with limited information (*13*−*15)*. Very recently, the three-dimensional structures of recombinant HRPC and its complex with BHA were analyzed by X-ray crystallography at 2.15 and 2.0 Å resolution, respectively (*16*, *17*). These studies and results obtained with mutated enzyme and by MD (*18*, *19*) indicate that the closest amino acid residue to BHA is Phe179 and that bound BHA forms a network of hydrogen bonds with His42, Arg38, and Pro139. However, HRPC complexed with smaller aromatic donors such as phenols was not analyzed, and comparative studies with other peroxidases to clarify the reason for the nonspecificity of donors are necessary.

After the first report of the X-ray crystallographic structure of CCP in 1980 (*20*), several other peroxidases, including lignin peroxidase (*21*), manganese peroxidase (*22*), ARP (*23*), *Coprinus cinereus* peroxidase (*24*), ascorbate peroxidase (*25*), peanut peroxidase (*26*), and barley grain peroxidase (*27*), were analyzed. Of these peroxidases, ARP is particularly interesting. Although ARP and HRPC belong to different classes within the plant peroxidase superfamily, i.e., class II and class III, respectively (*28*), these two enzymes resemble each other with respect to kinetic and structural properties (*28*−*36*). We therefore selected ARP as the most appropriate enzyme for comparison with HRP, which has been studied extensively.

We first analyzed ARP in a complex with iodide by X-ray crystallography and found that the iodide is located at the entrance of the access channel 12.8 Å from the heme iron (*37*). The electron transfer from the iodide to the ferryl oxide of the heme appears to cover the 7.8 Å to His56. The crystal structure of ARP−BHA complex was then determined at 1.6 Å resolution (*38*). The work presented here extends our study to the X-ray analysis of binding of SHA to ARP and compared it with the findings for MPO−SHA (*39*). Although we tried to locate the phenols in the ARP−phenols complex, no definite electron density for phenols was found, probably due to their low affinity for ARP. Therefore, we used the MD technique to locate several phenol compounds on the basis of the location of SHA as determined by X-ray crystallography. The heme iron−proton distances were examined by NMR relaxation. Furthermore, the rate constants of the reduction of cpds I and II by BHA and SHA were determined for HRPC and ARP with a stopped-flow apparatus.

Quantum chemical treatments for the redox reactions were investigated by Marcus and colleagues (*40*, *41*), and recently, the theory has been applied by several groups to the peroxidase-catalyzed reactions. At the end of this paper, our results are discussed in relation to the quantum chemical mechanism of electron transfer.

Table 1: Summary of Data Collection and Crystallographic Refinement

(A) Conditions and Results of Data Collection	
wavelength (Å)	1.5418
oscillation angle of IP (deg)	1.2
exposure time of IP (min)	30
no. of IPs	60
resolution limit (Å)	1.9
no. of measured reflections	119252
no. of independent reflections	24996
completeness (%)[a]	93.9
R_{merge} (%)[b]	4.3
(B) Results of Crystallographic Refinement	
resolution range (Å)	7.0−1.9
no. of refined atoms[c]	2767 (207)
no. of reflections ($F > 2\sigma_F$)	24343
R-factor (%)	16.3
R-free (%)	22.8
root-mean-square deviations from ideal values	
bond distances (Å)	0.019
angle distances (Å)	0.051
planar groups	0.023
chiral volumes (Å^3)	0.129
torsion angles of ω (deg)	3.0

[a] After the intensities of the equivalent reflections had been scaled and averaged, those where $F < \sigma_F$ were rejected. [b] $R_{merge} = \Sigma_h\Sigma_i|I_{hi} - \langle I_h\rangle|/\Sigma_h\Sigma_i\langle I_{hi}\rangle$. [c] Numbers in parentheses are the number of water molecules.

MATERIALS AND METHODS

Materials. ARP was crystallized as described previously (*42*). ARP used for other experiments was provided by T. Amachi of Suntory Co. The Reinheit Zahl (A_{403}/A_{280}) was 2.63. The concentration of the enzyme was determined spectrophotometrically from the molar extinction coefficient of 1.09×10^5 cm^{-1} M^{-1} at 405 nm (*30*). HRPC (type VII, RZ = 3.1, and type I, RZ = 1.2) was purchased from Sigma (St. Louis, MO). The enzyme concentration was determined spectrophotometrically from the extinction coefficient of 1.02×10^5 cm^{-1} M^{-1} at 403 nm (*43*). H_2O_2 and guaiacol were purchased from Wako (Osaka, Japan). Deuterium oxide (>99.85% pure) was purchased from the Commissariat l'Energie Atomique (Grenoble, France).

X-ray Crystallography of the ARP−*SHA Complex.* The crystals of ARP in a complex with SHA were prepared by soaking native ARP crystals for 10 h in 20 mM ammonium acetate buffer (pH 5.5) containing 25 mM SHA and 33% saturated ammonium sulfate. The crystals belong to space group $P4_22_12$ having one ARP molecule in the asymmmetric unit with the following cell dimensions: $a = b = 74.4$ Å and $c = 117.0$ Å.

Diffraction data for the complex crystal were collected at 1.9 Å resolution at room temperature on an R-AXIS IV imaging plate area detector. X-rays generated with a Rigaku rotating anode at 40 kV and 100 mA were focused with double-bent mirrors. The diffraction data recorded in each imaging plate were read out at 100 μm intervals and then processed using PROCESS (*44*). Intensities of the partial reflections recorded on two adjacent imaging plates were combined to obtain the integrated intensities. The conditions and results of data collection are shown in Table 1A.

The atomic parameters of ARP at pH 7.5 and 1.9 Å resolution (PDB file name 1ARP) (*23*) were used to initiate the structural refinement; several water molecules near the heme were excluded from the analysis. The parameters were refined by using the observed diffraction data of the complex with XPLOR (*45*). The $2F_o - F_c$ and $F_o - F_c$ maps, in which F_c and the phase angles were calculated with the resultant parameters, clearly localized the SHA molecule. An SHA model was fitted manually to the maps with TURBO-FRODO (*46*) and an IRIS 4D RPC^2 computer graphics system. The occupancy of SHA was assumed to be 1.0. The locations of water molecules were revised by alternate cycles of XPLOR refinement and inspection of the $2F_o - F_c$ and $F_o - F_c$ maps. In the refinement presented here, the *O*-glycoside moiety attached to Ser339 was located. The final model contains 207 water molecules in addition to the protein and SHA. The results of crystallographic refinement are shown in Table 1B. The mean coordinate error was estimated to be approximately 0.2 Å from a Luzatti plot.

Molecular Dynamics. Complex structures of ARP with several aromatic donors were estimated by MD with Insight II/Discover (Biosym/MSI, San Diego, CA) (*47*). The initial structure of ARP with each aromatic donor was constructed on the basis of the X-ray coordinates of the ARP−SHA complex. Each aromatic donor was placed manually in the heme cavity of resting ARP (PDB file name 1ARP) in reference to the spatial position of SHA in the ARP−SHA complex defined by X-ray crystallography. After removal of the X-ray-defined water molecules that collided with the aromatic donor, artificial solvent water molecules were added to the heme cavity of the complex within the region less than 20 Å from the heme iron. The calculation was based on the extensive systematic force field, which is very accurate for organometallic compounds (*47*). To confirm the validity of the MD approach, we first attempted to predict the ARP−SHA complex structure. The initial structure model of ARP−SHA was constructed by manual docking of SHA to the resting ARP as described above. After the structures were predicted with various restraints, we determined the condition that yielded the structure that best approximated the X-ray coordinates of the ARP−SHA complex as follows. No restraint was applied to the ARP side chain atoms which were exposed to the entrance edge, heme cavity, atoms of the heme and aromatic donors, and all the water molecules in the initial structure with exception of the distal water molecule located between the heme iron and His56 Nϵ. Cα atoms of the residues exposed around the heme were tethered with a quadratic force constant of 50. All of the ARP atoms except those mentioned above were tethered with a quadratic force constant of 85. The quadratic force constant for tethering in the Discover software varies from 0 to 100, indicating the atom is not tethered or tethered completely. In addition, distance restraints were applied to the oxygen atom of the distal water molecule. The distance between the oxygen atom and the Fe or His56 Nϵ was restrained to less than 3.5 Å. The corresponding water molecule (W364) was also observed between the heme iron and His56 Nϵ in the X-ray crystallographic structure of the ARP−SHA complex. After minimization of the energy of the initial structure, MD was performed at 300 K for more than 20 ps until the potential energy of the structure reached equilibrium. The ARP structure for interaction with each aromatic donor was predicted under the same conditions. A snapshot of the representative local minimum structure of each simulation was considered as a candidate for the ARP structure that interacts with appropriate aromatic donors. For the asymmetrical aromatic donors, resorcinol and *o*- and *m*-cresol, two initial structures were formed for each donor. After the MD simulation, the donor structure that positioned the phenolic oxygen closest to the heme iron was adopted.

NMR Measurements. Proton NMR measurements were performed essentially as described previously with a Bruker AMX-400WB NMR spectrometer at 298 K (*8*). Samples dissolved in deuterated phosphate buffer (100 mM) were analyzed in an NMR microtube (0.2 mL) with symmetric geometry along the B_0 field (*48*). The pH was measured in an NMR microtube with a Horiba model F-23 pH meter equipped with a low-impedance long and thin (3.2 mm × 180 mm) combination glass electrode (Sanwai Kagaku, Tokyo, Japan). The pH was calibrated with standard aqueous (H_2O) buffer, and the isotope effect was disregarded for the deuterated solutions. All the parameters were fitted by nonlinear least-squares methods unless otherwise stated. T_1 values were obtained by a standard inversion recovery method followed by a nonlinear three-parameter fitting method, and K_d values were obtained from UV−vis difference spectra. T_{1b} and T_{1f} were derived from a set of observed T_1 values (*8*) with the following equation:

$$1/T_1 = [E_0/(K_d + S_0)](1/T_{1b} - 1/T_{1f}) + 1/T_{1f} \quad (5)$$

where T_{1b} and T_{1f} are the spin−lattice relaxation bound to and free from ARP, respectively, E_0 and S_0 are the initial concentrations of ARP and aromatic donor, respectively, and K_d is the dissociation constant for dissociation of the aromatic donor from ARP. The value of T_{1b} was then transferred to T_{1M} using the relationship

$$1/T_{1b} = (1/T_{1M}) + (1/T_{1b}^*) \quad (6)$$

where T_{1M} is the relaxation time of aromatic donor protons due to the paramagnetic iron of ARP and T_{1b}* is the extent of induced relaxation enhancement due to the binding of aromatic donor to a large molecule. T_{1b}* was obtained from a diamagnetic ARP-CN, which was generated by mixing 50 mM KCN with 0.3 mM ARP. T_{1M} is related to the distance r between the heme iron and donor protons according to the Solomon−Bloembergen equation (*49*, *50*):

$$1/T_{1M} = [2\gamma_I^2\gamma_S^2S(S+1)/(15r^6)][3\tau_C/(1+\omega_I^2\tau_C^2) + 7\tau_C/(1+\omega_S^2\tau_C^2)] \quad (7)$$

where γ_I and γ_S are gyromagnetic ratios of the proton and electron, respectively, S is the spin quantum number of the heme iron, ω_I and ω_S are Larmor frequencies of the proton and electron, respectively, and τ_C is the correlation time. In this system, we could safely assume that $S = {}^5/_2$, $\omega_I^2\tau_C^2 \ll 1$, and $\omega_S^2\tau_C^2 \gg 1$ (*51*). Then eq 7 reduces to (*52*)

$$r = (8.66 \times 10^{-31} \times 1/T_{1M}^*\tau_C)^{1/6} \text{ cm} \quad (8)$$

If it is assumed that $\tau_C = 5 \times 10^{-11}$ s (*29*, *30*), eq 8 is further simplified to

$$r = (4.33 \times 10^{-41} \times 1/T_{1M})^{1/6}\ \text{cm} \quad (9)$$

Thus, the distance between the donor protons and the heme center is calculated from the observed values for T_1 for a set of aromatic donor protons.

Optical Difference Spectra. Optical difference spectra (enzyme and donor vs enzyme) were recorded in a Beckman DU650 spectrophotometer as described previously (*53*). Titrations were carried out at pH 7.4 in 50 mM sodium phosphate buffer at 25 °C. The enzyme concentration was 7−10 μM, and the substrate concentration was 0.5 μM to 50 mM. The cyanide-ligated form was prepared in the presence of 2 mM KCN. The dissociation constant, K_d, was calculated by a nonlinear least-squares method with the equation

$$\Delta A = \Delta\epsilon\{K_d + E_0 + S_0 - [(K_d + E_0 + S_0)^2 - 4E_0S_0]^{1/2}\}/2 \quad (10)$$

where S_0 and E_0 are the initial concentrations of the substrate and enzyme, respectively, K_d is the dissociation constant, ΔA is the absorbance for the peak minus that of the trough, and $\Delta\epsilon$ is the difference in molar absorbance. When $S_0 \gg E_0$, the following equation was used

$$\Delta A = \Delta\epsilon E_0S_0/(K_d + S_0) \quad (11)$$

That is,

$$1/S_0 = (\Delta\epsilon/K_d)(E_0/\Delta A) - 1/K_d \quad (12)$$

Usually, two individual experiments were performed, and the mean value is shown.

Kinetic Studies. Transient-state experiments were performed on an Applied Photophysics SX-17MX stopped-flow reaction analyzer equipped with a 1 cm cuvette, by mixing equal volumes of two solutions at 25 °C. For the stopped-flow experiments, one drive syringe contained the aromatic substrate and buffer [0.1 M phosphate buffer (pH 7.4)], and the second drive syringe contained cpd I or cpd II. Both syringes contained potassium nitrate (0.1 M). Usually, three to five runs were accumulated, and pseudo-first-order rate constants (k_{obs}) were calculated by one-exponential curve fitting. From the k_{obs} values obtained at three different substrate concentrations (10, 30, and 60 μM), the k_2 and k_3 values were calculated and expressed as the mean ± standard deviation.

HRP cpd I was prepared by adding 1 equiv of H_2O_2 to the resting enzyme (*55*). The reduction of HRP cpd I with substrate was followed at 411 nm, which is the isosbestic point between HRP cpd II and the resting enzyme. For the formation of ARP cpd I, a fresh preparation of ARP was preincubated with 1 equiv of H_2O_2 and allowed to stand until the resting form was recovered. One equivalent of H_2O_2 was furthermore added. The reduction of ARP cpd I with aromatic substrate was followed at 414 nm, which is the isosbestic point between cpd II and the native enzyme. HRP cpd II was prepared by adding 1 equiv of H_2O_2 and 1 equiv of $K_4Fe(CN)_6$ to a fresh enzyme solution, and the rate of its reduction with aromatic substrate was obtained at 423 nm, which is the isosbestic point between cpd I and the resting state. ARP cpd II was prepared from ARP cpd I by adding 1−1.2 equiv of $K_4Fe(CN)_6$ and used immediately in the reaction with the aromatic substrate. k_{obs} for the reaction was measured from the decrease in absorbance at the isosbestic point (426 nm) between the resting state enzyme and cpd I (*36*).

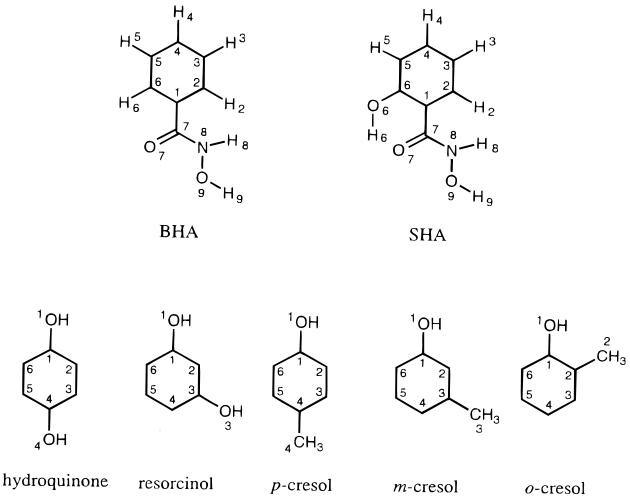

FIGURE 1: Atom numbering of BHA, SHA, hydroquinone, resorcinol, and *p*-, *m*-, and *o*-cresol molecules used in the text.

The rate of the steady-state reactions was measured in a Beckman DU650 spectrophotometer with guaiacol as a hydrogen donor in 33 mM sodium phosphate buffer (pH 7.4) at 25 °C. The concentrations that were used were 100 μM for guaiacol, 270 μM for H_2O_2, 5 nM for enzyme, and 1−1000 μM for hydroxamic acids. The initial increase in optical density at 470 nm was taken to calculate the rate (*56*).

RESULTS

Binding of Aromatic Donors to ARP Probed by Optical Difference Spectroscopy. We previously reported that, with respect to the optical difference spectrum patterns of HRPC−donor versus HRPC, aromatic donor molecules are divided into two groups (*54*). One group (termed type I), which includes *p*-cresol and phenol, undergoes a hypsochromic shift in the Soret band of HRPC, and the other group (termed type II), comprising donors such as resorcinol and guaiacol, is characterized by a bathochromic shift in the Soret band. BHA (Figure 1) had a type II-like change in the Soret region of the enzyme, a noticeably low K_d value, and a 3 order of magnitude difference in the extinction coefficient. Therefore, we classified BHA as type III (*54*). The difference spectrum of SHA was examined under the same conditions used to analyze BHA (Table 2). It is interesting that the K_d value of the HRPC−SHA complex is approximately 30 times larger than that of the HRPC−BHA complex.

In this study with ARP, the optical difference spectra of aromatic donors (*p*-cresol, resorcinol, BHA, and SHA) were observed in a similar manner, and the peak wavelength, the trough wavelength, K_d values, and $\Delta\epsilon$ values are also listed in Table 2. It is noteworthy that *p*-cresol, which has a type I spectrum for HRP, was converted to type II in the binding to ARP and that the K_d values of BHA and SHA for ARP increased 700- and 20-fold, respectively, compared with those for HRPC. Table 2 also shows that cyanide barely affected the binding of resorcinol and *p*-cresol in accordance

Table 2: Dissociation Constants of SHA, BHA, and Phenol Complexes with Resting ARP and Cyanide-Ligated ARP

		difference spectrum						
enzyme	donor	max (nm)	min (nm)	max (nm)	type[a]	K_d (mM)	$\Delta\epsilon$ (mM^{-1} cm^{-1})	ref
ARP	*p*-cresol	N[b]	381	410	II	58	11.0	this paper
ARP	resorcinol	N	382	411	II	22	9.0	this paper
ARP	BHA	N	378	409	III	3.2	66	this paper
ARP	SHA	N	381	409	III	3.2	49	this paper
ARP-CN	*p*-cresol	N	N	429	II′	86	1.3	this paper
ARP-CN	resorcinol	N	N	429	II′	27	0.86	this paper
HRPC	*p*-cresol	378	404	423	I	3.5	4.9	*54*
HRPC	resorcinol	N	N	411	II	6.7	3.0	*54*
HRPC	BHA	N	376	408	III	0.0046	51	this paper
HRPC	SHA	N	375	408	III	0.17	58	this paper
HRPC-CN	*p*-cresol	N	N	425	II′	5.7	3.7	*54*
HRPC-CN	resorcinol	N	N	425	II′	7.8	3.2	*54*
HRPC-CN	BHA	N	N	–	II′	0.15	–	*58*
HRPC-CN	SHA	N	N	428	II′	0.28	1.4	this paper

[a] See Hosoya et al. (*54*) for the definition of types I, II, III, and II′. [b] N means that no peak and no trough were found in the regions.

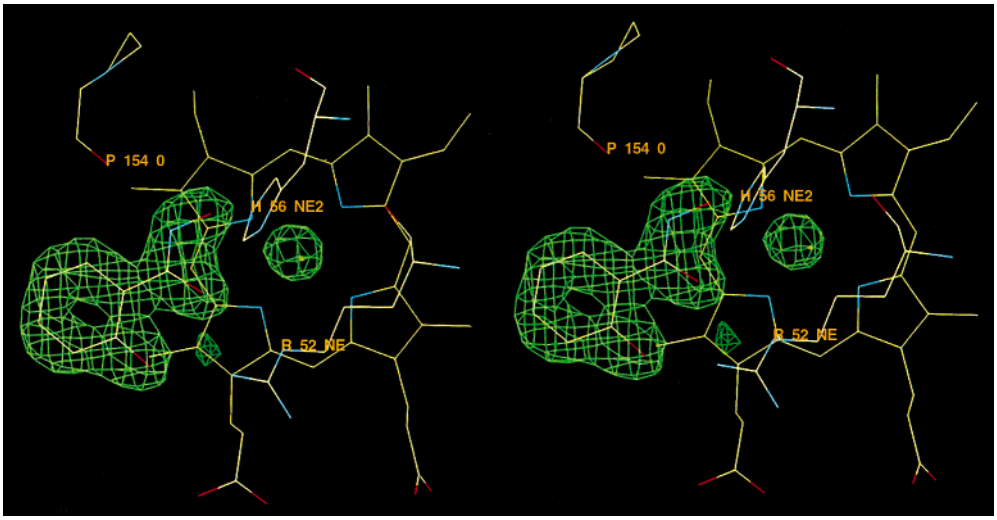

FIGURE 2: $F_o - F_c$ omit map of the SHA-bound form of ARP superimposed on the final model. The F_c and phase angles were calculated from the aromatic parameters except those of SHA and the solvent molecules.

with the observation reported for HRPC (*54*), but it does affect the binding of hydroxamic acids, especially BHA. It should be noted that the spectra were not affected by iodide (not shown). This is explained by the fact that the iodide binding site is at the entrance of the access channel on the distal side of the heme (*37*) and is distinct from the binding sites for aromatic donor molecules. Furthermore, the difference spectra for cyanide-ligated enzymes coincided with those for the resting enzymes.

Location of SHA in the Active Center of ARP Determined by X-ray Crystallography and MD. This X-ray analysis determined the crystal structure of the ARP−SHA complex at 1.9 Å resolution. The difference Fourier map (Figure 2) exhibits significant electron density, which clearly indicates the conformation and orientation of SHA. This map also shows the location of a solvent molecule at the distal side of the heme iron.

The mode of SHA binding to ARP is shown in Figure 3. Comparison with the structure of the ARP−BHA complex (*38*) reveals that the location of SHA in the active site is similar to that of BHA. The SHA molecule is located in the cavity on the distal side. The aromatic ring of SHA is accommodated in a hydrophobic region created by the heme pyrrole ring D and nearby hydrophobic amino acids (Ala92, Pro156, Leu192, and Phe230). The hydroxamic acid group of SHA is located in the distal cavity and is hydrogen-bonded to His56, Arg52, and Pro154 (Figure 3). The additional hydroxyl group of SHA relative to BHA does not form hydrogen bonds with any amino acid residues in the heme cavity. The distance from the heme iron to the center of the aromatic ring (ϕ) for the ARP−SHA complex is similar to that for the ARP−BHA complex (*38*) (Table 3).

The dihedral angle between the aromatic ring of BHA or SHA and the heme plane in the X-ray analysis was about 16−18° (Table 4).[2] This inidicates that the aromatic rings are nearly parallel to the heme plane, and the benzene rings of BHA and SHA are close to C18-CH_3 of the heme plane (Table 4 and Figure 4), which was first found in the HRPC−BHA complex by means of NOE (*8*, *11*).

It was reported that in the MPO−SHA complex, the SHA molecule displaces three of four water molecules from the distal heme pocket of the native enzyme (*39*). In the ARP−SHA complex, six water molecules (W417, W624, W625, W626, W675, and W723) were replaced by one SHA

[2] In the previous study (*38*), the dihedral angle between the heme D ring and the aromatic ring of BHA was calculated to be 9°.

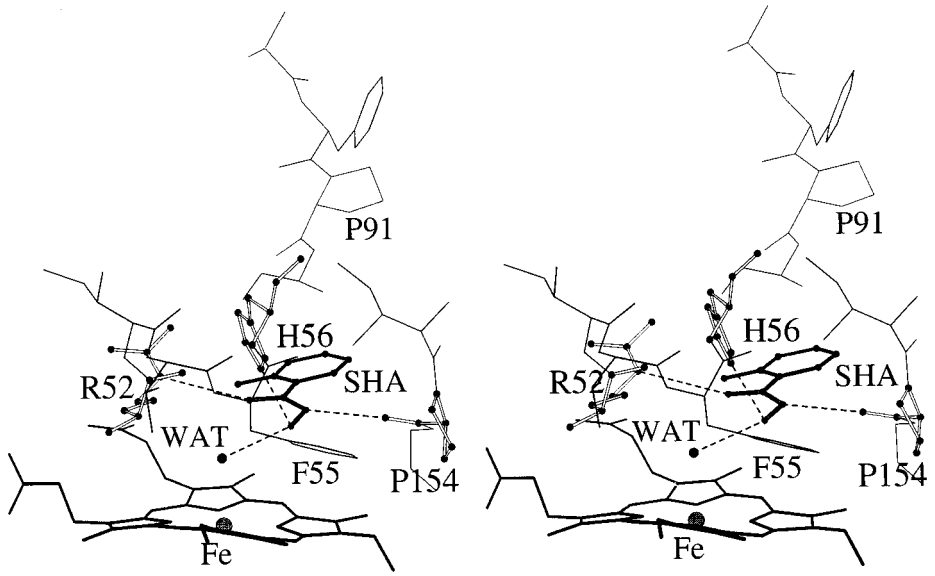

FIGURE 3: Closeup view of the environment of the heme group in the ARP−SHA complex obtained by X-ray crystallography viewed parallel to the heme plane.

Table 3: Distances between the Heme Iron and the Atoms of SHA and BHA Obtained by X-ray Analysis, NMR Relaxation, and Molecular Dynamics

			distance (Å) from the heme iron											
line	substrate	technique	C1	C2 H2[a]	C3 H3[a]	C4 H4[a]	C5 H5[a]	C6 H6[a]	O6	C7	O7 H7[a]	N7 H8[a]	O8	ϕ[b]
1	BHA	X-ray[c]	6.6	7.6	8.8	9.1	8.3	7.0	−	5.4	4.9	5.3	4.4	7.8
2	BHA	X-ray[c]	−	*7.6*	*9.7*	*10.1*	*8.8*	*6.5*	−	−	−	*6.0*	*3.5*	−
3	BHA	NMR[d]	−	*8.3*	*10.1*	*10.3*	*10.1*	*8.3*	−	−	−	−	−	−
4	BHA	MD[e]	9.2	9.5	10.5	11.9	11.6	10.3	−	7.9	7.9	6.8	5.5	10.5
5	BHA	MD[e]	−	*8.9*	*11.3*	*12.9*	*12.4*	*10.4*	−	−	−	−	−	−
6	SHA	X-ray[c]	6.9	7.8	9.1	9.5	8.9	7.6	7.1	5.6	5.1	5.3	4.4	8.2
7	SHA	X-ray[c]	−	*7.8*	*10.0*	*10.7*	*10.0*	−	−	−	−	*6.2*	*3.5*	−
8	SHA	MD[e]	8.5	9.0	10.4	11.4	11.0	9.7	9.7	7.2	7.3	6.2	5.0	9.9
9	SHA	MD[e]	−	*8.5*	*10.8*	*12.4*	*11.8*	−	−	−	−	*6.4*	*4.5*	−

[a] Data concerning hydrogen atoms are expressed in italic numbers. [b] ϕ denotes the center of the benzene ring. [c] Taken from Itakura et al. (*38*) and this paper. The italicized numbers are for the distance between the heme iron and the hydrogen atoms attached to C atoms. [d] Taken from Sakurada et al. (*8*). [e] Obtained via the MD procedure as described in Materials and Methods.

molecule, and two water molecules (W416 and W686) were shifted to W465 and W365, respectively (Figure 4). W365 in the complex lies between the distal histidine and the heme iron; the W365−iron distance is 2.8 Å. W365 is connected to O(9) of the SHA molecule via a hydrogen bond.

The binding of BHA or SHA to ARP was also examined by the MD method under various conditions as described in Materials and Methods. One of these conditions yielded the locations most similar to those obtained by X-ray analysis (Table 3), but the locations of both the BHA− and SHA−ARP complexes evaluated by MD are shifted outward as compared with the X-ray structures. Therefore, the distances O(7)−Arg52 Nϵ, N(8)−Pro154 O, and O(9)−His56 Nϵ were too great for the formation of hydrogen bonds. This discrepancy may be due in part to the lack of stabilization energy that involves hydrogen bond formation, which was disregarded in the MD procedures.

Location of Phenol Analogues in the Active Center of ARP As Examined by MD. The *p*-cresol and resorcinol complexes of ARP were analyzed by X-ray analysis in a manner similar to that used for the ARP−SHA and ARP−BHA complexes. The aromatic donors, however, were not found in electron density maps most likely due to the low affinity of these compounds for ARP (Table 2). Therefore, we studied the locations of these compounds on the enzyme by modeling and the MD method. The aromatic donors that were used

Table 4: Dihedral Angles and Distances between the Benzene Ring of Donors and the Heme Plane, or His56

		dihedral angle[a]	distance[b] (Å)			
donor	technique	(deg)	i	ii	iii	iv
BHA	X-ray[c]	18	4.1	6.7	3.3	2.7
BHA	MD[d]	32	6.7	7.6	4.8	4.3
SHA	X-ray[c]	16	4.3	6.7	3.4	2.7
SHA	MD[d]	23	6.3	7.1	4.4	3.8
hydroquinone	MD[d]	12	4.2	7.5	4.8	4.1
p-cresol	MD[d]	18	3.8	6.4	4.5	4.1
m-cresol	MD[d]	35	5.0	9.2	7.1	5.6
o-cresol	MD[d]	14	3.7	4.5	2.2	2.9
resorcinol	MD[d]	7	3.9	6.2	3.5	2.6

[a] Dihedral angles between the heme plane and the benzene ring of substrates. [b] i represents the distance between the center of the donor benzene ring and $C18H_3$, ii that between the oxygen atom of the hydroxy group of the donor and the center of the pyrrole D ring, iii that between the oxygen atom of the hydroxy group of the donor and the oxygen atom of Fe^{IV}=O, and iv that between the oxygen atom of the hydroxy group of the donor and the Nϵ of His56. The spatial position of the ferryl oxygen atom of ARP was estimated on the basis of the Fe−O distance in CCP's X-ray coordinates (*57*). [c] Obtained by X-ray analysis. [d] Obtained via the MD procedure as described in Materials and Methods.

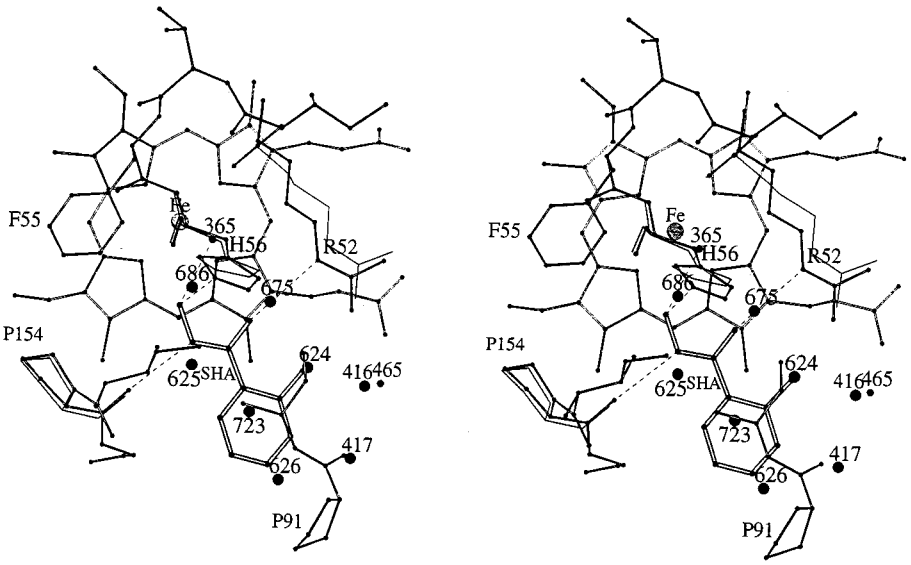

FIGURE 4: Closeup stereoview of the superposition of the models of the SHA-bound form and the native form. Balls and sticks represent the residues and the heme group of the SHA-bound form, and the thin bonds represent the three residues (R52, H56, and P154) in the native form. Large circles represent the water molecules in the native form that are replaced by the SHA molecule, while two small circles (W365 and W465) represent the water molecules found in the SHA-bound form. Possible hydrogen bonds involving SHA are depicted as broken lines. The hydrogen bond distances are as follows: O(7)−Arg52 Nϵ, 3.3 Å; N(8)−Pro154 O, 2.9 Å; O(9)−His56 Nϵ, 2.7 Å; and O(9)−W365, 2.6 Å. The Fe−W365 and Fe−O(9) distances are 2.8 and 4.3 Å, respectively.

Table 5: Distances between the Heme Iron and C or H Atoms of Aromatic Donors[a]

		distance from the heme iron (Å)												
substrate	technique	C1	C2 H2[d]	C3	C4 H4[d]	C5 H5[d]	C6 H6[d]	O1	O4	O3	M4[b]	M3	M2	ϕ[c]
hydroquinone	MD[e]	6.3	6.3	6.8	8.5	6.5	7.5	5.5	9.7	−	−	−	−	7.4
p-cresol	MD[e]	6.1	6.2	7.4	8.5	8.4	7.4	5.3	−	−	9.9	−	−	7.3
m-cresol	MD[e]	8.9	9.5	10.8	11.5	10.7	9.5	7.8	−	−	−	11.7	−	10.1
o-cresol	MD[e]	4.2	4.4	5.7	6.5	6.3	5.2	3.4	−	−	−	−	4.0	5.3
resorcinol	MD[e]	5.7	6.2	6.5	7.6	8.1	7.5	4.9	−	8.5	−	−	−	6.9
resorcinol	MD[e]	−	*6.5*	−	*9.6*	*8.1*	*6.0*	−	−	−	−	−	−	−
resorcinol	NMR	−	*9.2*	−	*9.4*[f]	*10.0*	*9.4*[f]	−	−	−	−	−	−	−

[a] The structures of ARP−donor complexes were obtained by MD. [b] M denotes the C atom of the methyl group. [c] ϕ denotes the center of the benzene ring. [d] Data concerning hydrogen atoms are expressed in italic numbers. [e] Obtained via the MD procedure as described in Materials and Methods. [f] Indicating that either one is the case (*8*).

include hydroquinone, resorcinol, *p*-cresol, *m*-cresol, and *o*-cresol. MD data, including the distances from the heme iron to the carbon and oxygen atom, and the centers of the benzene rings of these donors derived by MD procedures, are listed in Table 5. The dihedral angles between the benzene rings and the heme plane are listed in Table 4. It is interesting that the dihedral angles of these five donors vary from 7° (resorcinol) to 35° (*m*-cresol). On the basis of these results, we hypothesized that these small donors enter the crevice with various binding modes.

Determination of Proton−Iron Distances via an NMR Relaxation Experiment. Previously, we used the NMR relaxation method to determine the distances from the heme iron to protons of aromatic donors bound to HRPC (*8*). The proton−iron distances in ARP−donor complexes obtained by a similar method are listed in Tables 3 and 5. As seen in Table 3, the NMR relaxation data generally agree with those of X-ray analysis of the ARP−BHA complex, except an approximately 2 Å difference in the H6 of BHA. The proton−iron distances of the complex obtained by X-ray analysis are similar to those obtained by MD (lines 7 and 9 in Table 3).

An NMR relaxation experiment was performed only for resorcinol as a representative. Comparison of the MD data with the NMR data (Table 5) shows that the H4 value obtained with MD is similar to that obtained with NMR, but revealed that those for H2 and H6 are 3 Å closer to the heme iron.

Difference NOE spectra were obtained with various irradiation powers applied alternatively to the heme methyl protons and offset position, and intensity differences in the protons of aromatic donors at various irradiation times (10−500 ms) were observed. The difference NOEs were observed on the protons of aromatic donors irrespective of which heme methyl protons were irradiated. These results indicate that there is a nonselective spin diffusion between protons in the ARP−resorcinol complex, but the contribution of this nonselective NOE was less than $^1/_5$ of that of the selective NOE generated by irradiation at the 87 ppm resonance (peak *a*). We concluded that these results were valid for the qualitative assessment of the proximity between heme methyl and aromatic donors. Peak *a* was assigned tentatively to 3-methyl protons (*37*) following the assignment to *C. cinereus* peroxidase (*31*). Nevertheless, the results presented

Table 6: Reduction Rate Constants of Cpd I and Cpd II of ARP and HRPC for Reduction by BHA, SHA, *p*-Cresol, and Resorcinol

	$k_2 \times 10^{-6}$ (M^{-1} s^{-1})		$k_3 \times 10^{-6}$ (M^{-1} s^{-1})	
substrate	ARP	HRPC	ARP	HRPC
BHA	2.3 ± 0.2	5.2 ± 0.5	1.1 ± 0.1	3.0 ± 0.1
SHA	9.2 ± 0.4	1.4 ± 0.2	3.19 ± 0.03	1.2 ± 0.1
p-cresol	3.9[a]	42 ± 2[b]	nd[c]	1.06 ± 0.02[d]
resorcinol	11[a]	8.0 ± 0.9[b]	nd[c]	0.352 ± 0.003[d]

[a] Mean values of two experiments. [b] Values reproted in ref *62*. [c] Not determined. [d] Values reported in ref *55*.

here for NOE are inconsistent with the findings that the protons of BHA (*37*) and SHA (Figure 3) are closer to the 8-methyl than to the 3-methyl protons of the heme. Most likely, this is due to erroneous assignment of peak *a* obtained for *C. cinereus* peroxidase because the amino acid sequences of the two peroxidases are identical except for an additional N-terminal Gly in *C. cinereus* peroxidase. The same technique was applied to give a result consistent with the assignment of 8-methyl protons (*8*).

Rate Constants of the Oxidation Reactions for BHA, SHA, and Other Aromatic Donors with Compounds I and II of ARP and HRP. Due to the high-affinity binding of BHA to HRP (*58*) and its inhibitory action on the oxidation of guaiacol (*59*), BHA was considered a competitive inhibitor of HRP. However, it was also reported that BHA was oxidized in addition to the usual donor molecules during catalysis of HRP (*60*) and lactoperoxidase (*59*). In 1981, Aviram (*60*) reported the k_3 value for HRP, but this value was obtained with steady-state measurements, based on the assumption that $k_2 \gg k_3$. In the study presented here, the reduction rates for HRPC cpd II and ARP cpd II with BHA and SHA were obtained using a stopped-flow method (Table 6). The reduction rates (k_2) of HRP cpd I and ARP cpd I with BHA and SHA were also measured (Table 6). For a comparison, the reduction rates (k_2 and k_3) of cpd I and cpd II with *p*-cresol and resorcinol are included in Table 6, although these data were obtained under slightly different conditions.

The k_2 and k_3 values for BHA and SHA had a similar order both for ARP and for HRP, indicating that the $k_2 \gg k_3$ assumption is not correct for these donors. The k_2 and k_3 values for ARP are greater in SHA than in BHA, and the reverse is found in HRP. Similar results were obtained for k_2 and k_3 values measured with *p*-cresol and resorcinol. The k_2 and k_3 values for ARP with resorcinol were larger than those with *p*-cresol, and the relative magnitude was reversed for HRP values. An additional hydroxyl group in SHA and resorcinol may contribute to this phenomenon, although the exact cause is not clear. In contrast with the results for BHA and SHA, the k_2 values for *p*-cresol and resorcinol were found to be 20−40 times greater than the k_3 values for HRP.

The inhibitory action of BHA on the oxidation of guaiacol catalyzed by HRPC and ARP was tested with a steady-state method (*56*). Plots of the activities revealed that the concentrations of BHA causing half-inhibition were approximately 15 μM for ARP and approximately 55 μM for HRPC.

DISCUSSION

To date, only three X-ray crystallographic analyses of aromatic donor complexes with peroxidases, the MPO−SHA complex (*39*), the ARP−BHA complex (*38*), and the HRPC−BHA complex (*17*), have been reported. The results presented here for ARP−SHA were compared with the previous findings. The similarity of the ARP−SHA complex to the ARP−BHA complex (*38*) is clear. Both the aromatic rings are 7−9 Å from the heme iron, the distance for SHA being approximately 0.55 Å greater than that for BHA, and both are surrounded by hydrophobic amino acid residues at the entrance of the heme cavity. Both hydroxamic acid side chains extend inside the cavity, forming hydrogen bonds with His56, Arg52, and Pro154. The aromatic rings of BHA and SHA are nerely parallel with the heme plane, the dihedral angles being approximately 17°. The dissociation constants of the complexes also are similar to each other; both are on the order of millimolar.

The mode of BHA binding to HRPC (*17*) is similar to that of SHA in ARP−SHA and that of BHA in ARP−BHA. In HRPC−BHA, BHA forms hydrogen bonds to the catalytic histidine and arginine residues (His42 and Arg38) at the distal side of the heme and to the three-dimensionally conserved proline residue (Pro139). Moreover, a water molecule is located just above the heme iron in HRPC−BHA as is the case in ARP−SHA and ARP−BHA, and the water−iron distance in HRPC−BHA (2.6 Å) (*17*) is comparable to that in ARP−SHA (2.8 Å) and that in ARP−BHA (2.7 Å) (*38*).

Nevertheless, the mode of binding of BHA to HRPC differs from that of SHA or BHA to ARP in the following ways. (i) The hydrogen bond partner of the carbonyl oxygen of the aromatic donor molecule is the Nη atom of Arg38 in HRPC−BHA, whereas it is the Nϵ atoms of Arg52 in ARP−SHA and ARP−BHA. (ii) The water molecule closest to the heme iron atom is hydrogen-bonded to the carbonyl oxygen atom of BHA in HRPC−BHA, but in ARP−SHA and ARP−BHA, this water molecule is hydrogen-bonded to the hydroxamic hydroxyl groups of SHA and BHA.

The structure of the ARP−BHA complex is similar to that of the HRPC−BHA complex, whereas binding of SHA to ARP (Figure 3) or MPO (*39*) is different. The distances from the heme iron to the atoms of the benzene ring are 1−2 Å shorter in MPO−SHA than in ARP−SHA, indicating that the SHA molecule is more deeply embedded in the center of the pocket in MPO−SHA. The C1−C7 bonds are rotated 180° with respect to each other in the two complexes; SHA binds to MPO displacing three waters, one of which (W1) is positioned most closely to the heme iron. The addition of SHA to ARP displaces two water molecules (W365 and W465), W365 being closer than W686 to the heme iron (2.8 Å).

The iron−water distance in the ARP−SHA complex is 2.8 Å, which is longer than the usual Fe−ligand distance. In the case of the HRPC−BHA complex, the Fe−water distance in the crystal is 2.6 Å (*17*), and a 6c-HS heme is formed in the solution and in the crystal (*61*). It should be noted, however, that the accuracy of the distance between the heme iron and the ligand is generally limited (about 0.2 Å). More quantitative studies of the correlation between the distance and the electron structure for a given ligand are needed.

It is generally accepted that the structure of protein−donor complexes will be most exactly elucidated by X-ray crystallography, but it is impossible to apply this method for proteins in which crystallization rarely occurs and with low

affinity for the substrate. MD calculations are used to provide structural models for those systems for which X-ray characterization is not possible (*63*, *64*). This method has already been applied to the structural models of cytochrome *c* peroxidase (*65*), and the MD-derived structure was compared to the structure determined by X-ray crystallography. In this study, we used the MD method to study the ARP−BHA and ARP−SHA complexes and to determine the conditions which provide reasonable locations for BHA and SHA. On the basis of the resulting conditions, we attempted to predict the location of the five phenols on ARP. This study with BHA and SHA shows that MD procedures could provide results comparable to those of X-ray analysis (Table 3). We found that the benzene rings are trapped by the same hydrophobic amino acids at the entrance of the heme cavity, whereas the distances from Fe to the center of the rings of *m*-cresol and *o*-cresol are 2 Å longer and 3 Å shorter, respectively, than those of BHA and SHA. As for the dihedral angle between the benzene ring and the heme plane, the five donors showed values ranging from 7° to 35°, indicating that each donor can occupy a unique attitude in the heme cavity. These findings suggest that, in contrast to BHA and SHA molecules, the aromatic donors have significant freedom of movement in the heme cavity. This could be related to the fact that peroxidases in general exhibit low substrate specificity.

The distances between the heme iron and protons of the aromatic donors or the peptide amino acids were estimated by the NMR relaxation method (*8*, *53*, *66*). In this study, we compare these results with those of X-ray crystallographic analyses. The data presented in Table 3 demonstrate that the results of the two methods agree to within 1 Å. The slight difference in the distances between the heme iron and the protons of substrates may be ascribed to the use of the Solomon−Bloembergen equation under the assumptions of isotopic paramagnetic susceptibility and Boltzmann electron energy distribution (*53*, *67)*. In addition, the effect of zero-field splitting on the paramagnetic relaxation should not be disregarded (*68*−*70*).

As mentioned, the results obtained by means of NMR relaxation experiments closely agreed with those of X-ray analysis in the case of hydroxamic acids. However, there was a serious disagreement between the NMR data and the MD data for resorcinol. MD predicted that H6 in resorcinol is 0.5 Å closer to the heme iron than was H2, and NMR demonstrated that H2 is approximately 0.2 Å closer to the heme iron than H4/H6 (Table 5). This suggests that resorcinol adopts a revised orientation with respect to the heme. It should be noted that the distance *r* is calculated from an observed average relaxation rate of H4 and H6, and this rate is proportional to the average of the $(1/r)^6$ for each proton. Therefore, the distance to H4/H6 determined by NMR should be considered that from the closest adjacent proton. Misassigning H2 for H4/H6 is unlikely, and it is clear that H2 relaxes fastest in the presence of ARP and slowest in the absence of ARP. This indicates that H2 is positioned most closely to the heme iron. On the other hand, MD prefers an orientation which has more hydrogen bonds in the complex. The reversed orientation is rejected on the basis of an estimation of stabilized energy. Although further study is needed to explain these inconsistencies, it is possible that MD is not accurate enough to discern the orientation of resorcinol complexed with ARP in solution.

The ARP form that was used was the resting state and not one of the intermediates (cpd I and cpd II). It is likely, however, that the structure of the substrate binding site in the latter is similar to that in the native enzyme, because the tertiary structure of the enzyme is not influenced by the formation of the oxyferryl group, as seen in the cyanide-binding form of ARP (*34*) and in the cpd I form of CCP (*71)*. In addition, the dissociation constants of the aromatic substrates were found to be a few millimolar, being similar to the Michaelis−Menten constants (*7*). Therefore, it may be reasonable to assume that the electron transfer to the heme iron may occur essentially from the binding sites mentioned above, although donor molecules with a high kinetic energy are thought to oscillate strenuously at approximately equilibrated positions.

Electron transfer reactions can be described by the semiclassical Marcus theory (*40*, *41*), which can be summarized, for reactions between two centers held in a fixed distance, by the equation:

$$k_{et} = \frac{4\pi^2}{h} H_{AB}{}^2 \frac{1}{(4\pi\lambda RT)^{1/2}} \exp[-(\Delta G^\circ + \lambda)^2/4\lambda RT] \quad (13)$$

where k_{et} is the rate constant of the electron transfer reaction, ΔG° is the standard free energy change for the electron transfer, H_{AB} is the electronic coupling between the redox centers, h is Planck's constant, and λ stands for the nuclear reorganization energy which is defined as the energy required to distort the equilibrium geometry of the reactant state into the equilibrium nuclear geometry of the product state without electron transfer.

In the reaction between cpd II and a donor molecule, an electron in the HOMO of the latter is transferred to the LUMO of the heme of the former. The HOMO electron is practically 2pπ electrons of hydroxyl oxygen atoms of the aromatic donors (*55*), and the LUMO acceptor is considered to be the dπ−pπ orbital formed between the Fe and O atoms in cpd II (*72*). The MO energy of the latter has recently been calculated by Density Functional Calculation to be −3.4 eV (*72*). On the other hand, the HOMO energies of phenols were not calculated by this method, but we have the results obtained by ab initio calculation methods (*55*). The difference in energy at these levels should be related to the values for ΔG° in eq 13. The rate constant k_{et} is also affected by H_{AB} which is a function of the distance between and orientation of the redox centers. As shown in distance iii in Table 4, the distances between the hydroxyl oxygen atoms of aromatic donors and the oxygen atom of Fe^{IV}═O are on the order of 3−6 Å. These distances are shorter than those of CCP or cytochrome *c* system (*21*).

It is noteworthy that the dihedral angles between the heme plane and the benzene ring of phenols vary greatly (Table 4). This implies that these small substrate molecules can bind to the enzyme in various orientations and that a condition where there is a small dihedral angle with respect to the heme plane is not necessarily a prerequisite for a high rate of electron transfer.

It is well-known that peroxidases have various substrates (*1*, *2*). We previously reported that log k_3 values for an analogue of phenols and anilines correlate well with the HOMO energy levels (*55*). Because HOMO energy is related

to redox potentials and σ factors, the correlations of these values for analogues of phenols and indoleacetic acids with log k_2 and log k_3 have also been reported (*60*, *73*−*75*).

In the reaction between cpd I and a donor molecule, an electron in the HOMO of the donor molecule is transferred to the LUMO in the heme of cpd I. The ground state of cpd I is the a_{2u} π-cation radical state ($^4A_{2u}$) with a total spin of $^3/_2$ localized to the porphyrin ring ($S = {}^1/_2$) and the Fe^{IV}═O center ($S = 1$). The LUMO is β spin a_{2u} with −8.4 eV. This is approximately 5 eV lower than the LUMO of cpd II in accordance with the difference in rate constants. The overlap integral, another factor influencing the rate constant, is formed by the 2pπ orbital of the hydroxyl oxygen and the a_{2u} orbital that covers the heme plane. These orbitals are in closest proximity in the heme plane, and the distance between them is 3−6 Å as shown in Table 4.

Special attention should be given to the distance between the hydroxyl oxygens of the donors and the His56 of the enzyme because modification of His42 of HRPC (which corresponds to His56 of ARP) inhibits the reaction (*76*). Although it has not yet been confirmed that the electron transfer from the donor to the LUMO of the heme is mediated by His56, it is interesting to note that these distances are found to be of an order similar to those described above (Table 3) and that the electron transfer from iodide to Fe^{IV}═O of ARP seems to be mediated by His56 and hydrogen tunneling (*37*).

A quantitative study based on the spatial distributions of donors in the active center of ARP will lead to furthering our understanding of the electron transfer mechanism of peroxidase reactions.

ACKNOWLEDGMENT

We thank Ms. Yuko Hori for her technical assistance with NMR measurements, Dr. S. Okayasu for helpful discussions, and Dr. V. Fülop for providing the coordinates of CCP compound I.

REFERENCES

1. Saunders, B. C., Holmes-Siedle, A. G., and Stark, B. P. (1964) *Peroxidase*, Butterworths, Washington, DC.
2. Everse, J., Everse, K. E., and Grisham, M. B. (1991) *Peroxidases in Chemistry and Biology*, Vols. I and II, CRC Press, Boca Raton, FL.
3. Dunford, H. B., and Stillman, J. S. (1976) *Coord. Chem. Rev. 19*, 187−251.
4. Hosoya, T. (1960) *J. Biochem. (Tokyo) 47*, 794−803.
5. Santimone, M. (1974) *Can. J. Biochem. 53*, 649−657.
6. Dunford, H. B., and Cotton, M. L. (1975) *J. Biol. Chem. 250*, 2920−2932.
7. Patel, P. K., Mondal, M. S., Modi, S., and Behere, D. V. (1997) *Biochim. Biophys. Acta 1339*, 79−87.
8. Sakurada, J., Takahashi, S., and Hosoya, T. (1986) *J. Biol. Chem. 261*, 9657−9662.
9. Veitch, N. C. (1995) *Biochem. Soc. Trans. 23*, 232−240.
10. Smith, A. T., and Veitch, C. (1998) *Curr. Opin. Chem. Biol. 2*, 269−278.
11. Thanabal, V., de Ropp, J. S., and La Mar, G. N. (1987) *J. Am. Chem. Soc. 109*, 7516−7525.
12. Ortiz de Montellano, P. R. (1992) *Annu. Rev. Pharmacol. Toxicol. 32*, 89−107.
13. Banci, L., Carloni, P., and Savellini, G. G. (1994) *Biochemistry 33*, 12356−12366.
14. Smith, A. T., Du, P., and Loew, H. (1995) in *Nuclear Magnetic Resonance of Paramagnetic Molecules* (La Mar, G. N., Ed.) pp 75−93, Kluwer Academic Publishers, Dordrecht, The Netherlands.
15. Zhao, D., Gilfoyle, D. J., Smith, A. T., and Loew, H. (1996) *Proteins: Struct., Funct., Genet. 26*, 204−216.
16. Gajhede, M., Schuller, D. J., Henriksen, A., Smith, A. T., and Poulos, T. L. (1997) *Nat. Struct. Biol. 4*, 1032−1038.
17. Henriksen, A., Schuller, D. J., Meno, K., Welinder, K. G., Smith, A. T., and Gajhede, M. (1998) *Biochemistry 37*, 8054−8060.
18. Chang, Y.-T., Veitch, N. C., and Loew, G. H. (1998) *J. Am. Chem. Soc. 120*, 5168−5178.
19. Howes, B. D., Rodriguez-Lopez, J. N., Smith, A. T., and Smulevich, G. (1997) *Biochemistry 36*, 1532−1543.
20. Poulos, T. L., Freer, S. T., Alden, R. A., Edwards, S. L., Skoland, U., Eriksson, B., Xuong, N., Yonetani, T., and Kraut, J. (1980) *J. Biol. Chem. 255*, 575−580.
21. Poulos, T. L., Edwards, S. L., Wariishi, H., and Gold, M. H. (1993) *J. Biol. Chem. 268*, 4429−4440.
22. Sundaramoorthy, M., Kishi, K., Gold, M. H., and Poulos, T. L. (1994) *J. Biol. Chem. 269*, 32759−32767.
23. Kunishima, N., Fukuyama, K., Matsubara, H., Hatanaka, H., Shibano, Y., and Amachi, T. (1994) *J. Mol. Biol. 235*, 331−344.
24. Petersen, J. F. W., Kadziola, A., and Larsen, S. (1994) *FEBS Lett. 339*, 291−296.
25. Patterson, W. R., and Poulos, T. L. (1995) *Biochemistry 34*, 4331−4341.
26. Schuller, D. J., Ban, N., van Huystee, R. B., McPherson, A., and Poulos, T. L. (1996) *Structure 4*, 311−321.
27. Henriksen, A., Welinder, K., and Gajhede, M. (1998) *J. Biol. Chem. 273*, 2241−2248.
28. Welinder, K. G. (1992) *Curr. Opin. Struct. Biol. 2*, 388−393.
29. Kjalke, M., Andersen, M. B., Schneider, P., Christensen, B., Shülein, M., and Welinder, K. G. (1992) *Biochim. Biophys. Acta 1120*, 248−256.
30. Anderson, M. B., Hsuanyu, Y., Welinder, K. G., Schneider, P., and Dunford, H. B. (1991) *Acta Chem. Scand. 45*, 1080−1086.
31. Lukat, G. S., Rogers, K. R., Jabro, M. N., and Goff, H. M. (1989) *Biochemistry 28*, 3338−3345.
32. Veitch, N. C., Tams, J. W., Vind, J., Dalbϕge, H., and Welinder, K. G. (1994) *Eur. J. Biochem. 222*, 909−918.
33. Farhangrazi, Z. S., Copeland, B. R., Nakayama, T., Amachi, T., Yamazaki, I., and Powers, L. S. (1994) *Biochemistry 33*, 5647−5652.
34. Fukuyama, K., Kunishima, N., Amada, F., Kubota, T., and Matsubara, H. (1995) *J. Biol. Chem. 270*, 21884−21892.
35. Kunishima, N., Amada, F., Fukuyama, K., Kawamoto, M., Matsunaga, T., and Matsubara, H. (1996) *FEBS Lett. 378*, 291−294.
36. Abelskov, A. K., Smith, A. T., Rasmussen, C. B., Dunford, H. B., and Welinder, K. G. (1997) *Biochemistry 36*, 9453−9463.
37. Fukuyama, K., Sato, K., Itakura, H., Takahashi, S., and Hosoya, T. (1997) *J. Biol. Chem. 272*, 5752−5756.
38. Itakura, H., Oda, Y., and Fukuyama, K. (1997) *FEBS Lett. 412*, 107−110.
39. Davey, C. A., and Fenna, R. E. (1996) *Biochemistry 35*, 10967−10973.
40. Marcus, R. A. (1968) *J. Phys. Chem. 72*, 891−899.
41. Marcus, R. A., and Sutin, N. (1985) *Biochim. Biophys. Acta 811*, 265−322.
42. Kunishima, N., Fukuyama, K., Wakabayashi, S., Sumida, M., Takaya, M., Shibano, Y., Amachi, T., and Matsubara, H. (1993) *Proteins: Struct., Funct., Genet. 15*, 216−220.
43. Aibara, S., Yamashita, H., Mori, E., Kato, M., and Morita, Y. (1982) *J. Biochem. (Tokyo) 92*, 531−539.
44. Higashi, T. (1990) *PROCESS: A Program for Indexing and Processing R-AXIS IIc Imaging Data*, Rigaku Corp., Tokyo.
45. Brünger, A. T. (1992) *XPOLR Version 3.0: A System for X-ray Crystallography and NMR*, Yale University Press, New Haven, CT.

46. Roussel, A., and Cambillau, C. (1989) in *Silicon Graphics Germany Partner. Directory*, pp 77−78, Silicon Graphics, Mountain View, CA.
47. *Discover User Guide, October 1995*, Biosym/MSI, San Diego, CA.
48. Takahashi, S., and Nagayama, K. (1988) *J. Magn. Reson. 76*, 347−351.
49. Solomon, I. (1955) *Phys. Rev. 99*, 559−565.
50. Bloembergen, N. (1957) *J. Chem. Physiol. 27*, 572−573.
51. Wüthrich, K. (1976) *NMR in Biological Research: Peptides and Proteins*, North-Holland Publishing Co., Amsterdam.
52. Schejter, A., Lanir, A., and Epstein, N. (1976) *Arch. Biochem. Biophys. 174*, 36−44.
53. Burns, P. S., Williams, R. J. P., and Wright, P. E. (1975) *Chem. Commun.*, 795−796.
54. Hosoya, T., Sakurada, J., Kurokawa, C., Toyoda, R., and Nakamura, S. (1989) *Biochemistry 28*, 2639−2644.
55. Sakurada, J., Sekiguchi, R., Sato, K., and Hosoya, T. (1990) *Biochemistry 29*, 4093−4098.
56. Hosoya, T., and Morrison, M. (1967) *J. Biol. Chem. 242*, 2828−2836.
57. Fülop, V., Phizackerley, R. P., Soltis, S. M., Clifton, I. J., Wakatsuki, S., Erman, J., Hajdu, J., and Edwards, S. L. (1994) *Structure 2*, 201−208.
58. Schonbaum, G. R. (1973) *J. Biol. Chem. 248*, 502−511.
59. Kimura, S., and Yamazaki, I. (1979) *Arch. Biochem. Biophys. 198*, 580−588.
60. Aviram, I. (1981) *Arch. Biochem. Biophys. 212*, 483−490.
61. Smulevich, G., Feis, A., Indiani, C., Recucci, C. H., and Marzocchi, P. (1999) *J. Biol. Inorg. Chem. 4*, 39−47.
62. Job, D., and Dunford, H. B. (1976) *Eur. J. Biochem. 66*, 607−614.
63. McCammon, J. A., and Harvey, S. (1987) *Dynamics of Proteins and Nucleic Acids*, Cambridge University Press, Cambridge, U.K.
64. Kaptein, R., Boelens, R., Scheek, R. M., and van Gunstern, W. F. (1988) *Biochemistry 27*, 5389−5395.
65. Collins, J. R., Du, P., and Loew, G. H. (1992) *Biochemistry 31*, 11166−11174.
66. Modi, S., Saxena, P., Behere, D. V., and Mitra, S. (1990) *Biochim. Biophys. Acta 1038*, 164−171.
67. Jardetzky, O., and Roberts, C. C. K. (1981) *NMR in Molecular Biology*, Academic Press, New York.
68. Fukui, H., Miura, K., and Matsuda, H. (1990) *J. Magn. Reson. 88*, 311−319.
69. Sharp, R. R. (1993) *J. Chem. Phys. 98*, 6092−6101.
70. de Ropp, J. S., Mandel, P., Brauer, S. L., and La Mar, G. N. (1997) *J. Am. Chem. Soc. 119*, 4732−4736.
71. Edwards, S. L., Xuong, N., Hamlin, R. C., and Kraut, J. (1987) *Biochemistry 26*, 1503−1511.
72. Kuramochi, H., Noodleman, L., and Case, D. A. (1997) *J. Am. Chem. Soc. 119*, 11442−11451.
73. van Haandel, M. J. H., Rietjens, I. M. C. M., Soffers, A. E. M. F., Veegers, C., Vervoort, J., Modi, S., Mondal, M. S., Patel, P. K., and Behere, D. V. (1996) *J. Biol. Inorg. Chem. 1*, 460−467.
74. Candeias, L. P., Folkes, L. K., Porssa, M., Parrick, J., and Wardman, P. (1996) *Biochemistry 35*, 102−108.
75. Candeias, L. P., Folkes, L. K., and Wardman, P. (1997) *Biochemistry 36*, 7081−7085.
76. Bhattacharyya, D. Kr., Bandyopadhyay, U., and Banerjee, R. K. (1992) *J. Biol. Chem. 267*, 9800−9804.

BI982925L